Illumination system in visible-light with variable solar-divergence for the solar orbiter METIS coronagraph

M. Tordi*[a], M. Bartolozzi[a], S. Fineschi[b], G. Capobianco[b], G. Massone[b], S. Cesare[c]
[a]Space Technologies Srl, viale Combattenti A. d'Europa 9/G, 45100 Rovigo – Italy; [b]Osservatorio Astronomico di Torino, Via Osservatorio, 30, 10025 Pino Torinese TO – Italy; [c]Thales Alenia Space SpA - Strada Antica di Collegno, 10146 Torino

ABSTRACT

The measurement of the stray-rejection capabilities of METIS is part of the acceptance package of the instrument. The Illumination System in Visible Light (ISVL) has been developed to allow the stray-light rejection measurement down to $1x10^{-9}$ and under different operating conditions. The main characteristics of ISVL are outlined and discussed; the activities for the integration and verification of ISVL included the absolute radiometric characterization of the facility, including radiance measurement and radiance spatial and angular distribution. The procedures used to measure the performances of the facility are discussed and the obtained results illustrated.

Keywords: OGSE, illumination system, stray-light, coronagraphy

1. INTRODUCTION

The Multi-Element Telescope for Imaging and Spectroscopy (METIS) has been selected in 2009 by the European Space Agency as part of the payload of the Solar Orbiter mission [1], [2], [3]. The instrument allows the multiband imaging and UV polarimetry of the solar corona; the optical design of the telescope is based on an inverted occulter configuration, to minimize the thermal load entering into the instrument. Figure 1 shows a layout of the telescope, with the Inverted External Occulter (IEO) placed on the left.

The measurement of the radiance of the corona close to the Sun's disk from space-borne observatories requires a precise control of the instrumental stray-light. METIS has been designed to achieve a stray-light rejection level $B_{stray} < 10^{-9} \cdot B_{source}$ [4].

The achievement of the stray-light rejection capability of the instrument shall be confirmed by measurements performed on the flight model, which will take place at the Optical Payload Systems facility (OPSys) [5].

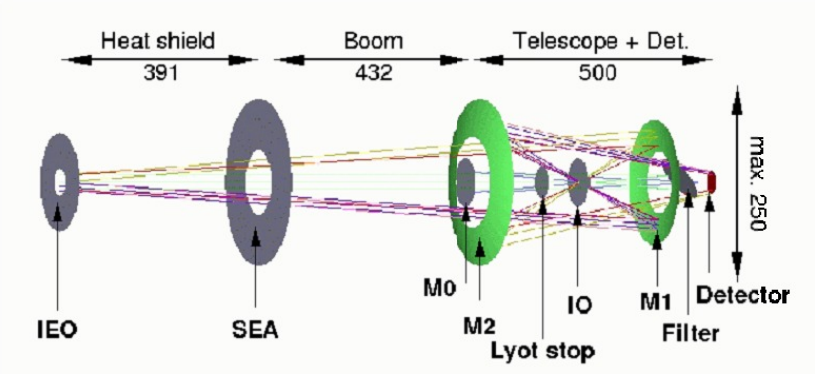

Figure 1 Optical layout of METIS.

* massimiliano.tordi@spacetechnologies.it; phone +39 0425 471055; fax +39 0425 471095; www.spacetechnologies.it

Solar Physics and Space Weather Instrumentation VI, edited by Silvano Fineschi, Judy Fennelly, Proc. of SPIE Vol. 9604, 96040V · © 2015 SPIE
CCC code: 0277-786X/15/$18 · doi: 10.1117/12.2207475

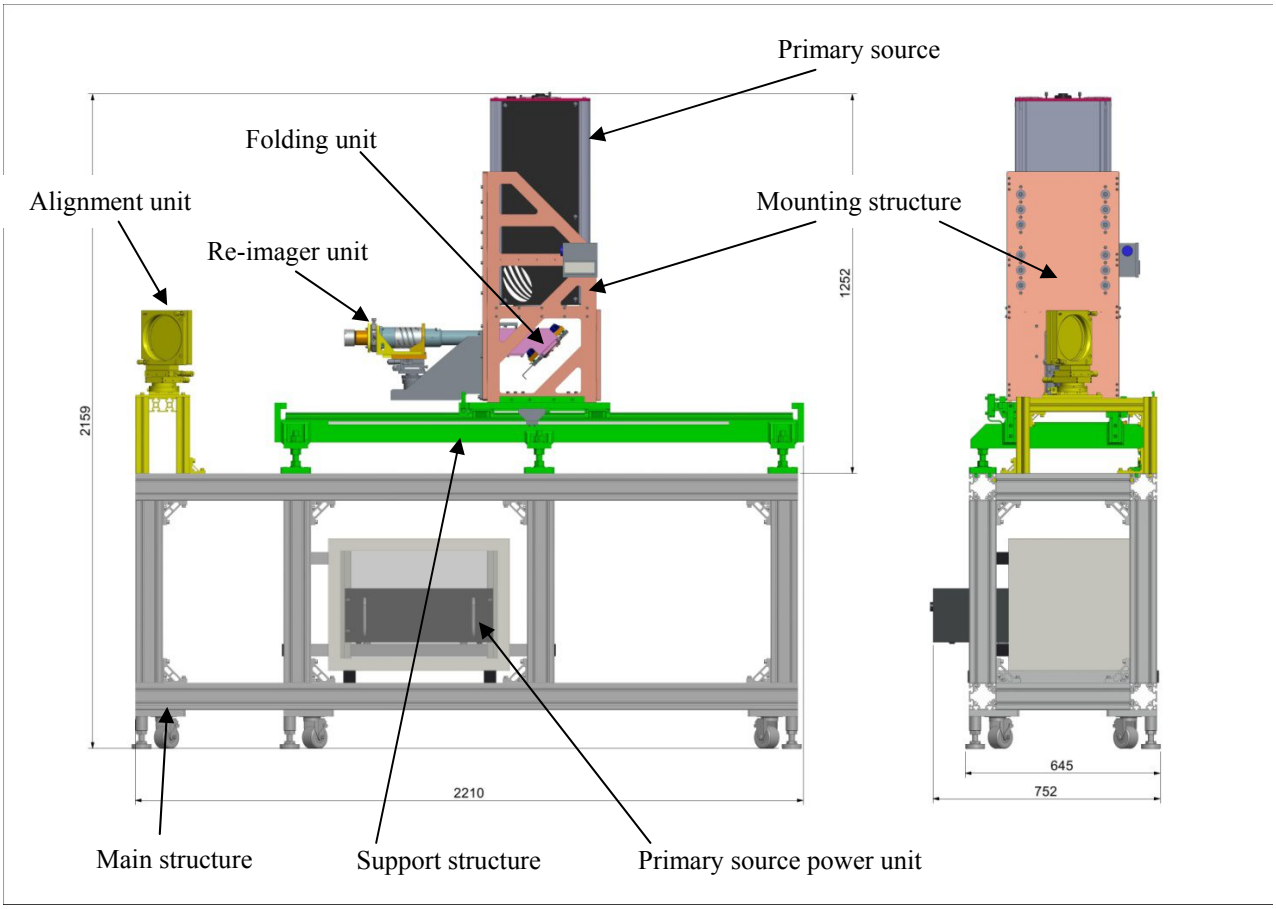

Figure 2 Layout of ISVL.

The execution of the measurement requires the design and integration of a visible light source (hereafter Illumination System in Visible Light, ISVL); this source, in combination with the off-axis parabola placed inside the OPSys vacuum pipeline, must generate a radiance pattern over the instrument external occulter with a radiance level high enough to guarantee the measurement of the residual stray-light of the instrument.

2. ISVL DESCRIPTION

The purpose of the ISVL system consists in providing a suitable visible light source to simulate the solar disk. The simulation of the solar disk allows the execution of two fundamental tests on METIS:

- Verification of the instrument stray-light rejection at different distances of the probe to the Sun
- Calibration of the vignetting function

ISVL shall be interfaced to SPOCC, the Space Optics Calibration Camera hosted by Altec S.p.a in Turin. The optical interface is represented by an off-axis parabola which sets the primary requirements for ISVL optical system.
Figure 2 shows the configuration of ISVL:

- The main structure is used to mount the whole system and to move it inside the operating area for preliminary alignment and it holds every other subsystem of ISVL.
- The support structure is used for the detailed alignment of the system; it holds the linear stage which is used to move the source in such a way to reproduce different operating condition (i.e. different Sun angular diameters).
- The translation stage holds four main sub-systems:

    - The main source, which is a Xenon short arc-lamp Superior Quartz Products, model SQP-SX30001 mounted inside lamphouse equipped with a dichroic ellipsoidal mirror. The lamphouse is provided by Science Tech Inc.
    - The folding unit, a flat folding mirror with a dichroic coating.
    - An interchangeable re-imager unit installed over an XYZ adjustment system (to adjust focus and decenter for internal alignment)
    - Every previously mentioned subsystem is mounted over the mounting structure, which sets the reference for internal alignment

  A magnetic relative encoder is used to place the carriage stage at the operating position after initial calibration. The magnetic strip is glued onto the support structure, while the sensor unit is attached to the carriage. The translation stage is used to move the system in such a way to reproduce the Sun angular diameter under different operating conditions (see below).
- The alignment mirror is a flat folding mirror mounted over a kinematic 2-axis stage and over two linear stages; it is used to fold the optical axis minimizing the polarization induced by the coatings and to save space inside the operating area. Its mount allows the accurate alignment of the system.
- The power unit of the primary source is placed inside the main structure and protected by a suitable enclosure.

Two re-imagers are used to properly operate ISVL, namely the IC re-imager (IC, infinite conjugated) and the FC re-imager (FC, finite conjugated). One re-imager provides the optical interface to SPOCC using the off-axis parabola in infinite-conjugated mode: a circular disk is illuminated by ISVL and it is placed at the focal plane of the parabola, which generates a collimated beam whose divergence gives the angular diameter of the Sun. Such configuration cannot be used to simulate the Sun at the closest distance reached by Solar Orbiter (0,28 AU), since the pipeline diameter is too small. It is then necessary to use a different procedure to simulate the disk at these distances. The parabolic mirror is used in finite conjugated mode: an annular aperture is optically conjugated by the parabolic mirror to the external occulter of METIS, thus illuminating the edge of the occulter, the f-ratio on the occulter giving the required angular diameter of the Sun. ISVL is thus equipped with a second interchangeable objective lens which gives the proper optical interface to the parabolic mirror. In order to vary the angular diameter of the simulated Sun in finite conjugated mode (FC) it is necessary to vary the distance of the parabolic mirror to the plane of the external occulter; this leads in cascade to several consequences:

- the annulus diameter shall change since the magnification changes while the diameter of the external occulter is fixed: ISVL is equipped with several interchangeable annular stops
- the distance of the annulus to the parabolic mirror shall change to give the proper conjugation: ISVL mechanics allows the translation of the source along an axis to achieve the required distance
- the f-ratio of the beam of light coming onto the parabola from ISVL shall change to avoid illumination of the internal surfaces of SPOCC: the FC lens objective allows the correction of the f-ratio

The same translation is also used to place the system in the correct position for the infinite conjugation use (IC).

3. ISVL INTEGRATION AND MAIN SUBSYSTEMS TEST

The integration and test of ISVL started at subsystem level after verification of the compliance of each part to the specifications defined at design level. After the completion of the integration and test of each sub-system the whole system has been integrated and tested.

Hereafter we will summarize the main tests performed at subsystem level and finally we will present the results of the tests performed over the whole system.

3.1 Main Structure and carriage

With regard to the Reference Coordinate System in Figure 3 the right rail was assumed as the one that lies on a smaller X-coordinate, and it was assumed to be the one that determines the translation accuracy of the ISVL carriage, while the other rail acts as a vertical support. As seen Figure 4, in order to align the carriage to the previously fixed right rail, an operation of backlash removal between the carriage and the two re-circulating ball runners of right rail was carried out (top-right). For this purpose, a couple of grub screws were added near these runners (left). Note that all four screws for all four runners must be loosen before acting on those grub screws.

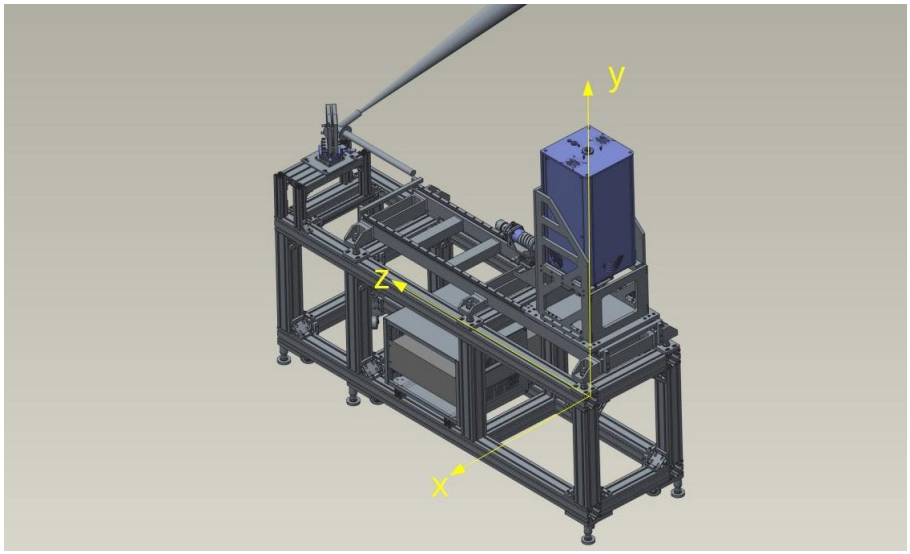

Figure 3 Reference Coordinate System for ISVL-TAV and ISVL-STA subsystems. Pitch is about X-axis, and yaw is about Y-axis.

Figure 4 The backlash between the runners on the right rail and the carriage was removed by grub screws. Then, the left rail was aligned by tighten up its screws as they were overtaken by the carriage sliding along its stroke (bottom-right).

Once this operation was completed, the ISVL carriage was positioned at one end of its stroke, and all the screws previously loosen were tighten up.

In order to estimate the machining, welding and mounting induced distortions, a measure of the vertical straightness deviation of each rail mounted on ISVL-STA frame was carried out. Then, straightness deviations not recoverable by joint adjustments were corrected by inserting calibrated shims between the rails and the underlying welded structure.

The measures were obtained by sliding the dial indicator holder base on the 1 m long granite inspection plate while the dial indicator head were in contact with the upper face of the rail. The measure were performed within the range allowed by the inspection table size and next to the screws, therefore with a fixed interval of 60 mm. The straightness of the remaining extension of the rails (0.68 m) was estimated by a curve fit. The survey took into account the relative inclination between the inspection plate and the rails.

As seen in Figure 6, the curves that terminate at the abscissa of 1000 are dial indicator readouts, while the curves that terminate at the abscissa of about 1600 are their parabolic fit extended to the whole length of the rail, minus the contribute of the tilt, that was calculated as the tilt of the segment through the extremes of the readouts parabolic approximation.

First of all, two independent measurements by dial indicator were performed, in order to evaluate the relative tilt between the inspection plate and the rail. With reference to Figure 6, these measurements are the curves named DX and DXagg1, and they appear to be very similar to each other. On the basis of DXagg1 data, a parabolic fit was calculated in order to estimate the tilt component of the measures. The curves named DX-tilt and DXagg1-tilt, barely distinguishable from each other, represent the measure minus the tilt.

The rest of the curves has been obtained by inserting shims of appropriate thickness to recover the required straightness. It is remarkable that the straightness achieved has been kept almost unchanged even after the transport of the entire structure by truck, from the laboratory in Rovigo to its final destination at OPSys, in Turin.

Figure 5 An adjustment of the vertical straightness deviations of the rails was carried out by means of repeated measurements at a distance of 60 mm and systematic insertion of shims. A 0.01 mm resolution dial indicator sliding on a 1 m long, DIN 876/0 class granite inspection table was used.

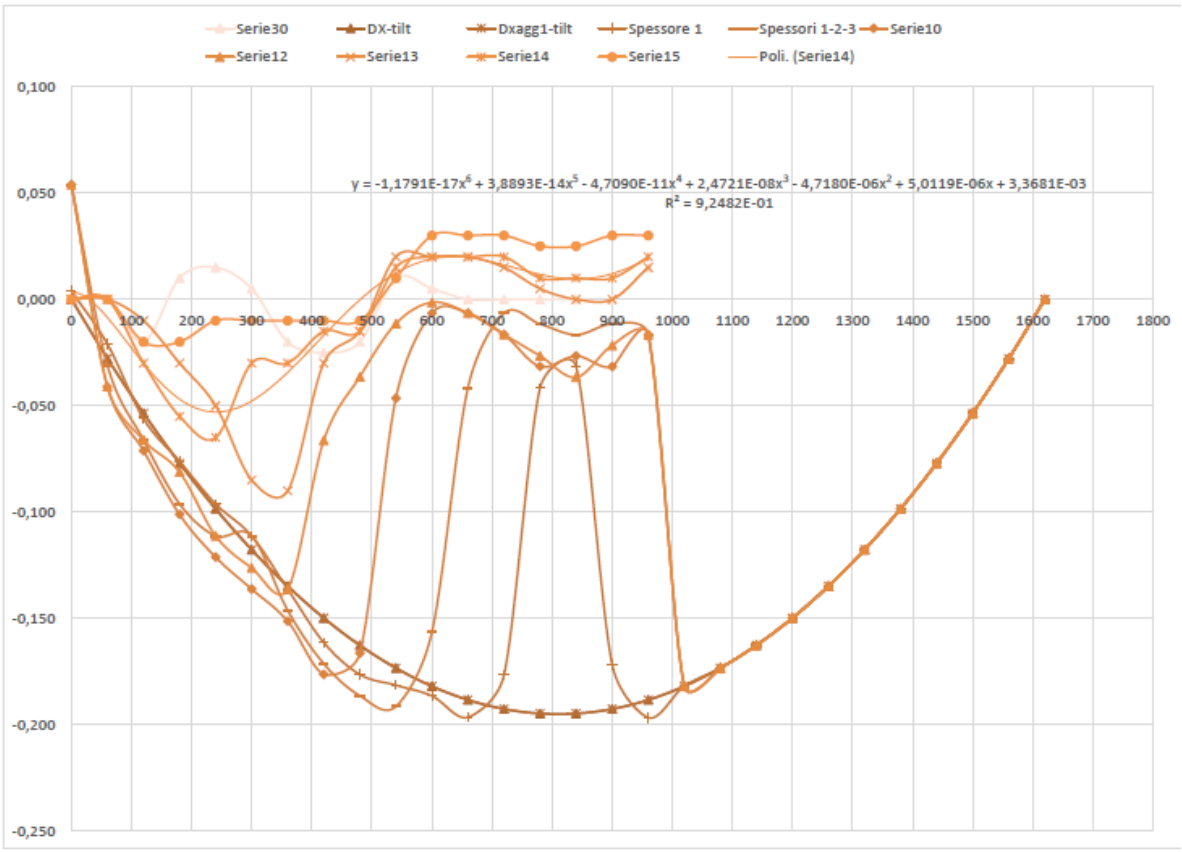

Figure 6 Measure and correction of the right rail sag. Units are mm. For the sake of clarity, only tilt-free curves are shown regardless the tilt was removed via software or via regulation screws adjustment. Measurements for the left rail show a similar behavior.

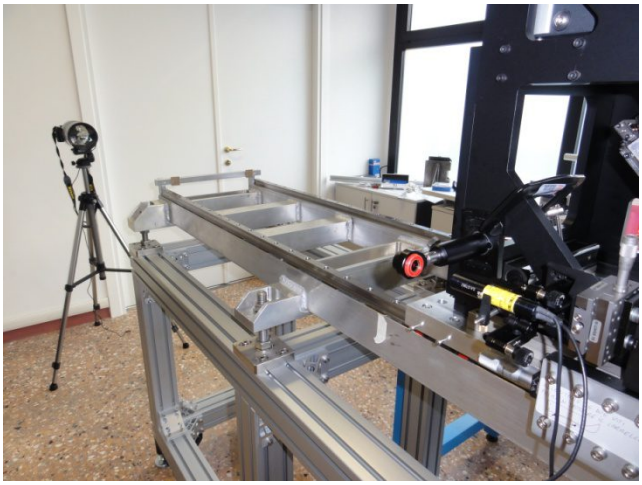

Figure 7 Optical setup utilized for the measurement of the angular deviation of the ISVL carriage along its stroke.

The straightness of the rails has been optically measured using the set-up shown in Figure 7. Initial adjustments to both laser and telescope positions were carried out in order to align the laser beam within the angular field of view of the camera and to keep it within the aperture of the telescope regardless the position of the carriage along its stroke.

In order to discriminate between yaw and pitch, the camera was leveled so that the horizontal and vertical displacements of the focused spot correspond to yaw and pitch rotations respectively. Because the carriage rails, the laser beam and the optical axis of the telescope was substantially parallel each other, roll isn't measured by this setup.

3.2 Re-imagers

The re-imagers of ISVL were assembled and tested in order to verify their compliance with the expected performances.

The FC re-imager is the most complicated one: it is made of three optical groups, namely a condenser unit, a magnification unit and a field unit. A sketch of the system is given in Figure 8. The central group is used to modify the magnification of the objective and its numerical aperture in image space. This is necessary as the objective is used in finite conjugation mode and its distance to the off-axis parabola placed inside SPOCC is varied according to the angular radius of the Sun that must be simulated; hence, to avoid the direct illumination of the vacuum chamber, the f-ratio in image space of the reimager must change, since the diameter of the off-axis parabola is of course fixed.

The group of lenses formed by lens L5 and L6 make this work and it is mounted onto a barrel that is translated along the main body of the camera to allow the variation of the magnification. The verification of this translation stage consists in:

- functional verification: the helicoidal rail shall allow a smoothed translation of the barrel inside the main body of the camera along the whole available stroke;
- play recovery: there must be no play among the mechanical parts.
- performance verification: the helicoidal rail shall allow the control of the barrel position with an accuracy better than 50μm;

The sleeve with helicoidal rails has three rails; the verification showed that the movement of the barrel was quite smooth at the center of the stroke, but it knocked out at the begging and at the end of it. To remove this problem the sleeve was dismounted and the rails were worked to ameliorate the translation of the screws heads inside of them.

A small quantity of Dow Corning SG10 vacuum-compatible grease was added, then the system has been re-assembled. The resulting translation of the barrel is perfectly smooth along the whole range. Two different plays exist within the system:

1. Play between the screw stem and the linear guide made on the main body of the camera
2. Play between the sleeve and the plate blocking plate used to mount the camera on and to _x the sleeve over the camera body.

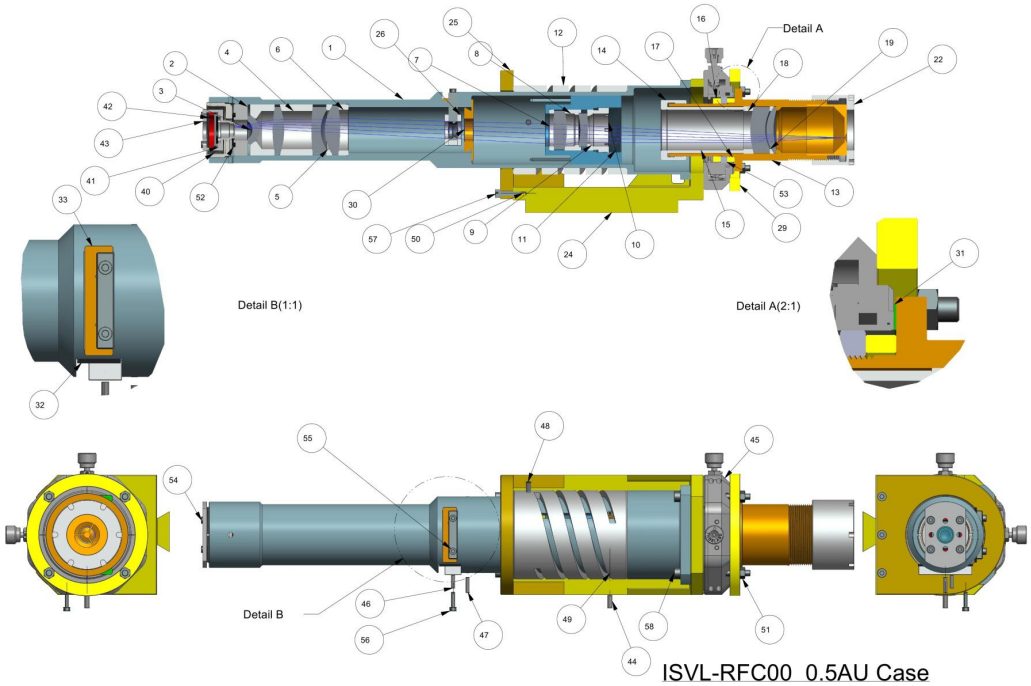

Figure 8 FC re-imager.

To remove the first type of play a small ring has been inserted between the screw and the linear rail, almost completely removing the play. For the second problem the play between the parts has been measured using a caliper, then a plate of suitable thickness has been inserted to recover the space between the parts.

A performance verification of the translation system has been performed with a caliper pressed onto a screw of the helicoidal rail and moving back and forth along the translation direction. The resulting sensitivity is close to the instrument accuracy (10μm).

The analysis of the point-spread-function has been performed by using the following set-up:

- a diode laser
- a fiber collimator
- a single mode fiber
- a fiber holder with a positioning system

The fiber collimator is used in reverse mode, i.e. the collimated beam emitted by the laser diode is focused onto the tip of the fiber mounted on the collimator. The alignment is achieved by maximizing the output power at the other end of the fiber. The single-mode fiber has a mode diameter of 4:5_m, which is small enough to allow the measurement of the point spread function. The first set of measurements gave the result shown in Figure 21: the image shows that the PSF was altered by large aberrations, mainly coma. Furthermore, it has been found that the a significant beam deviation occurred:

- First, a pinhole (diameter equal to 50μm) was mounted on the object plane of the re-imager, as close as possible to the center of the object plane
- Second, the best focus for the pinhole image was found
- Third, a stop with a small calibrated hole in its center was inserted exactly at the center of the image plane

It has been found that the stop blocked the light; the uncertainty on the pinhole position was not large enough to justify the observation, leading to the conclusion that at least one element was not properly mounted.

After careful inspection of the set-up, it has been necessary to dismount the optical system and to verify the correctness of the lens mountings. First, the lens group made of L5 and L6 has been dismounted and checked. It has been found that lens L6 was not properly aligned since the stop ring was not completely tighten. The ring has been tighten with the required torque and fixed. The doublet has been separately tested to verify its compliance to the design.

After the re-alignment of the L5 / L6 group the imager has been re-assembled and tested. Despite some improvement, yet the performances were below the design requirements. Careful inspection of the design and of the assembled system lead to the conclusion that the main source of the observed aberration depends on the misalignment of the third lens of the optical train. The mounting concept ("poker chips") is based on the assumption that a close _t between the spacers and the main body of the camera lead to the alignment of the lenses; to ease the centration of the lenses a wedge of suitable angle was foreseen on the spacers. Lens L3 has the largest radius of curvature and the inspection lead to the conclusion that the wedge was not steep enough to allow the centration of the lens. To solve this problem the following list of activities has been performed:

- disassembly of the camera
- definition of a mechanical set-up to mechanically center the lens onto the spacer:
    - measurement of the lens and spacer diameters
    - procurement of calibrated spacers to ensure the correct positioning of the lens w.r.t. the lens spacer
    - blocking of the lens-spacer-references assembly
    - gluing of the lens to the barrel at three points on the edge of the lens
    - after curing, remove of the references

After the successful completion of the above mentioned activities, the camera has been re-assembled and tested. The test results are perfectly in agreement with the Monte Carlo simulations obtained by introducing the prescripted tolerances.

3.3 Folding unit

The ISVL-FUN assembly was checked by itself about its angular stroke and minimum tilt variation that it can produce on the mirror by the regulation screws. For this purpose the assembly was placed onto an inspection plate and its mirror interface plate was made parallel to the inspection plate itself by means of a dial indicator. Then, one of the wedges was regulated at its limit position and the vertical distances of the plate was measured at opposite sides by the dial indicator. As seen in Figure 9 this distance was about 1.4 mm. Because the horizontal distance between the opposite positions of the dial indicator was about 150 mm, the resulting tilt was greater than 30'.

The parallelism error between the mirror interface plane and the opposite flexure pivot seat was also checked resulting in an error smaller than the 0.01mm dial indicator resolution.

In order to measure the minimum tilt the mount can produce on the mirror, the same dial indicator was placed at a point diametrically opposite to a wedge, while the latter was being finely adjusted by its regulation screw. The minimum vertical displacement was clearly smaller than 0.01mm, that corresponds to an angle of 26", so a value of about 15" can be reasonably assumed.

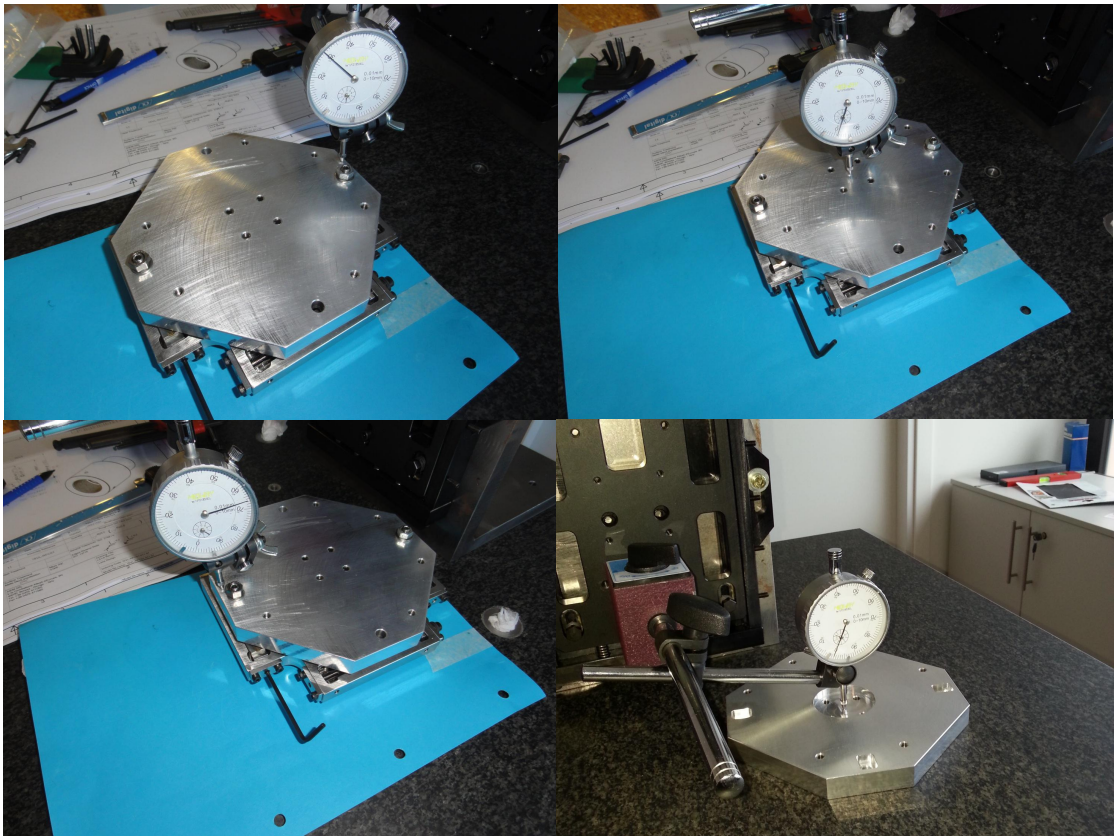

Figure 9 Measurement of the angular stroke for ISVL-FUN mirror plate. One wedge was regulated at its limit position, resulting in a vertical range of 1.4 mm for the plate. The distance between opposite dial indicator positions was about 150 mm, so the tilt range was greater than 30'. On bottom-right, the measured parallelism between the mirror interface plane and the opposite flexure pivot seat was smaller than the 0.01mm dial indicator resolution.

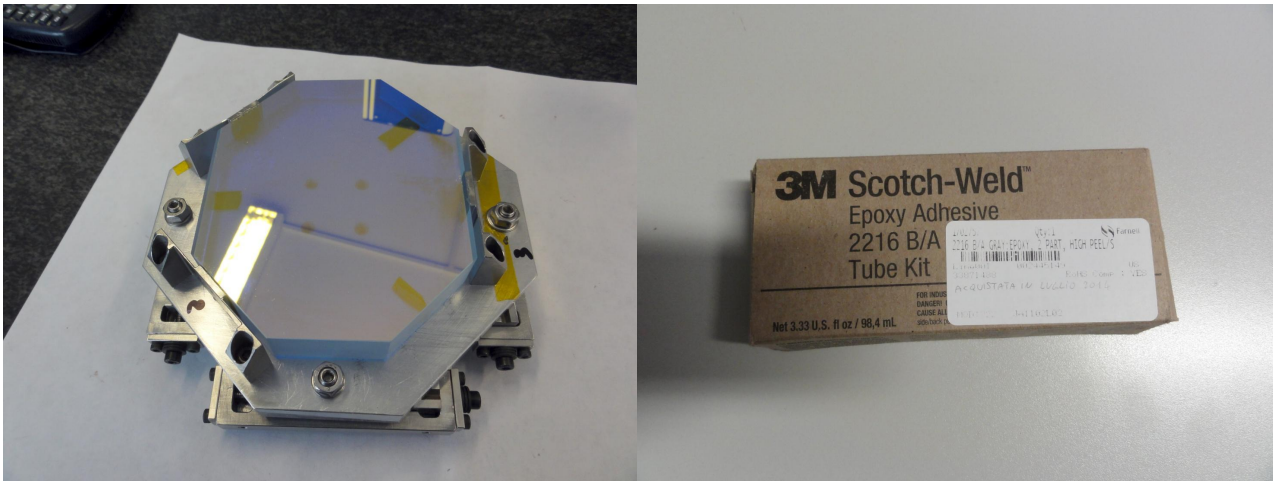

Figure 10 The flexures were bonded to the mirror, after the perpendicularity of the former was achieved by means of kapton film. A flexible, two-part, room temperature curing epoxy adhesive with high peel and shear strength was used (bottom).

4. SYSTEM LEVEL TEST

4.1 List of tests and test procedure

The tests performed on ISVL included the measurement of the radiance and the measurement of the radiance distribution.

Measurement of the radiance level

The following instrumentation has been used to measure the output flux:

- Ocean Optics Inc HR2000+ High Resolution Spectrometer Spectroscopy Software and Support
- Ocean Optics DH-2000 UV-VIS-NIR Light Source
- Thorlabs IS200 2" Integrating Sphere
- Integrating sphere, 6" LabSphere
- Thorlabs PDA 200 C Photodiode Amplifier
- Newport Optical Power Meter Model 1830C, 818-UV Detector, 883-UV, OD3 Attenuator
- Thorlabs ND40A Reflective Filter, ND=4.0

The following procedure is used to measure the flux:

- **Spectral response calibration – wavelength axis**
  The relationship between the wavelength value and the pixel position on the spectrum-photometer detector is usually obtained by fitting a polynomial to a set of measurements. The measurements are made by using a light source with known spectral features, i.e. with emission lines whose wavelength is known by the physical process on the basis of the emission.
- **Spectral response calibration – radiant flux / radiant flux density axis**
  After the calibration of the wavelength / pixel position relationship (horizontal axis), it is necessary to calibrate the vertical axis (counts / physical units). To this aim the following procedure is used:

    - A reference lamp is used to calibrate the spectral response of the spectrophotometer
    - A reference calibration spectrum is generated and used to convert the counts of the spectrometer into the appropriate radiometric units

  The limitation of this procedure is that while the reference lamp is interfaced to the spectrophotometer directly through a multi-mode fiber optic cable, the source under test must be measured using an integrating sphere and

interfacing the fiber optic to one of the exit ports of the integrating sphere itself. As the reflectance of the integrating sphere is not certified, while the whole sphere-detector assembly is, another step is necessary to performed the measurement.
A certified diode laser is used to fix the absolute radiometric scale: the laser diode flux at 632,8 nm is measure through the sphere / detector assembly and the result is used to fix the absolute radiometric scale.

Measurement of the radiance distribution

While the radiance value is an absolute measurement, the measurement of the radiance uniformity is a relative one. Different measurements are made for the IC and FC configurations.

The spatial uniformity measurement procedure and instrumentation for the FC configuration are the following. A pin-hole is made at a certain distance from the center of a stop placed on the re-imager. The flux is measured by rotating the stop held in place onto the optical system. The measurement is made using the integrating sphere–photodiode assembly.

To measure the angular uniformity in one shot, a telecentric microscope objective having real exit pupil is focused onto a pin-hole made at the image plane of the optical system; a camera is placed at the exit pupil plane of the microscope objective (see Figure 11 and Figure 12).

An image taken by the camera is a map of the angular distribution of the radiance. The angular resolution is given by:

$$\Delta\alpha = f \cdot p \tag{1}$$

f focal length of the objective
p pixel size of the camera

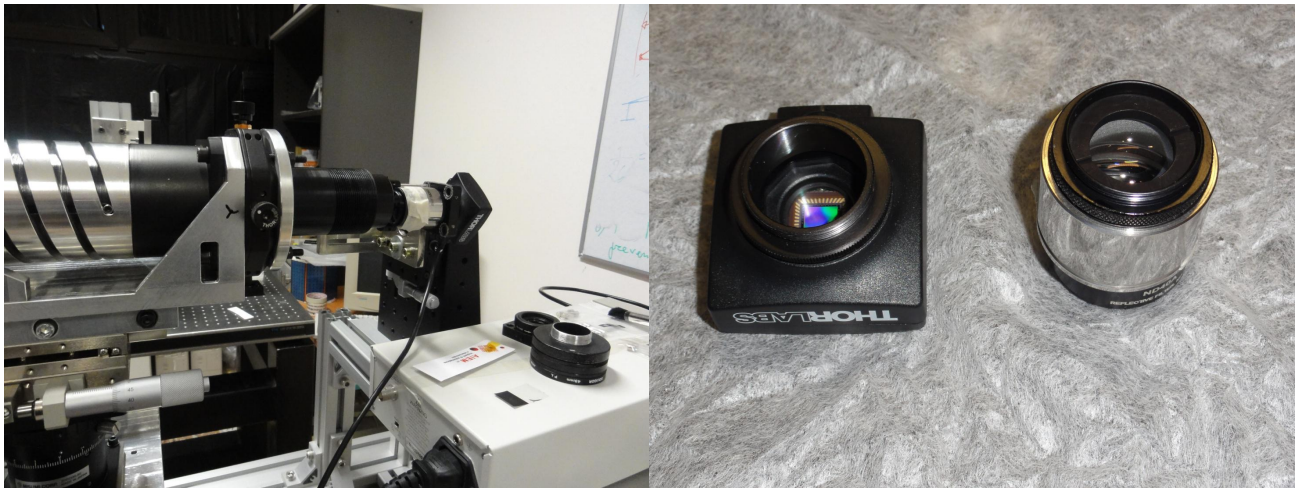

Figure 11 Measurement of the radiance uniformity in FC configuration; on the right, camera and objective used to measure the radiance uniformity.

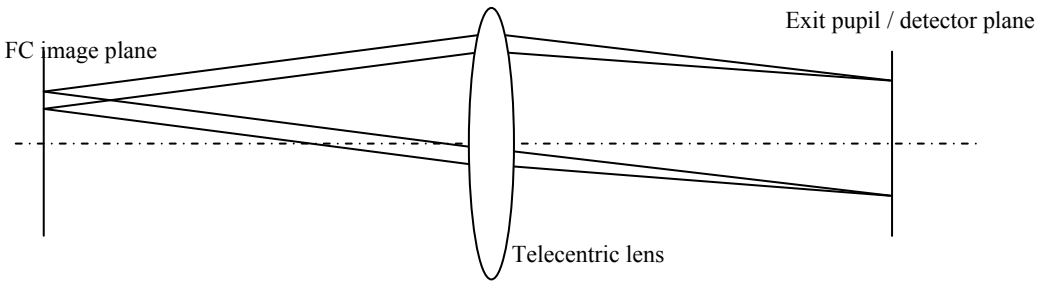

Figure 12 Uniformity measurement set-up.

The instrumentation used is a camera Thorlabs DCC1445M-GL, a telecentric lens objective Thorlabs LSM03-VIS EFL=39.1 LWD=25.9 and suitable spacers. A neutral density filter is also added to avoid the saturation of the camera.

A different approach is used for the IC configuration. The average of the angular uniformity of the IC configuration is the spatial uniformity at the inverted occulter of METIS, while its spatial uniformity is the angular uniformity at the inverted occulter.

The measurement of the spatial uniformity is made by using a pin-hole / neutral density filter / detector assembly, which is placed close to the stop of the re-imager. The flux is measured by sliding the pinhole held in place onto the optical system. The measurement is made using the photodiode assembly, without using the integrating sphere.

4.2 Test results

Figure 13 shows the flux spectral distribution once the calibration procedure is made. The power incident on the fiber placed at the exit port is obtained by integrating the spectrum within the required range (580 nm – 640 nm). The relationship between the measurement and the entrance flux is obtained using the theory of the integrating sphere, described in the following equations:

$$M = \frac{R}{1 - R(1 - f)} \tag{2}$$

$$L = \frac{P}{A_{fiber}\pi \cdot NA^2} \tag{3}$$

$$\Phi = \pi A_{sphere} \frac{L}{M} \tag{4}$$

The symbols have the following meaning:

M	integrating sphere constant
R	reflectance of the integrating sphere
f	ratio of the sum of the exit port and entrance port area to the area of the sphere
P	power measured on the tip of the fiber
L	radiance inside the integrating sphere
NA	numerical aperture of the fiber
A_{fiber}	area of the fiber core
A_{sphere}	surface area of the integrating sphere
Φ	flux at the entrance window

The results of the measurements are shown in Table 1.

Table 1. Radiance measurements, FC configuration.

Configuration	Measured flux	Flux at the IS entrance port	Equivalent mean radiance
0.5 AU	5.2 x 10^{-9} W	1.57 x 10^{-7} W	50.5 W/cm^2/sr
0.3 AU	3.4 x 10^{-9} W	1.03 x 10^{-7} W	49.1 W/cm^2/sr

Table 2. Radiance measurements, IC configuration.

Configuration	Measured flux	Equivalent mean radiance
1.0 AU	1.8 x 10^{-6} W	121 W/cm^2/sr
0.5 AU	7.0 x 10^{-7} W	47.0 W/cm^2/sr

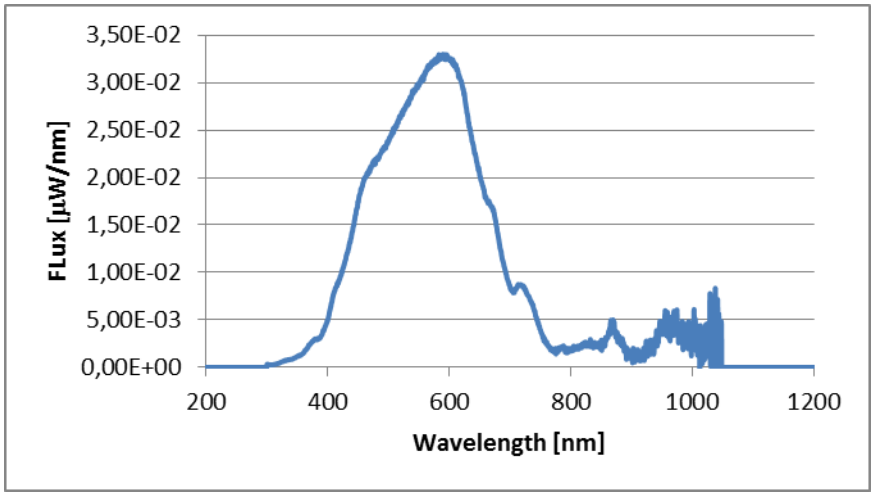

Figure 13 Flux spectral distribution measured with the calibrated system.

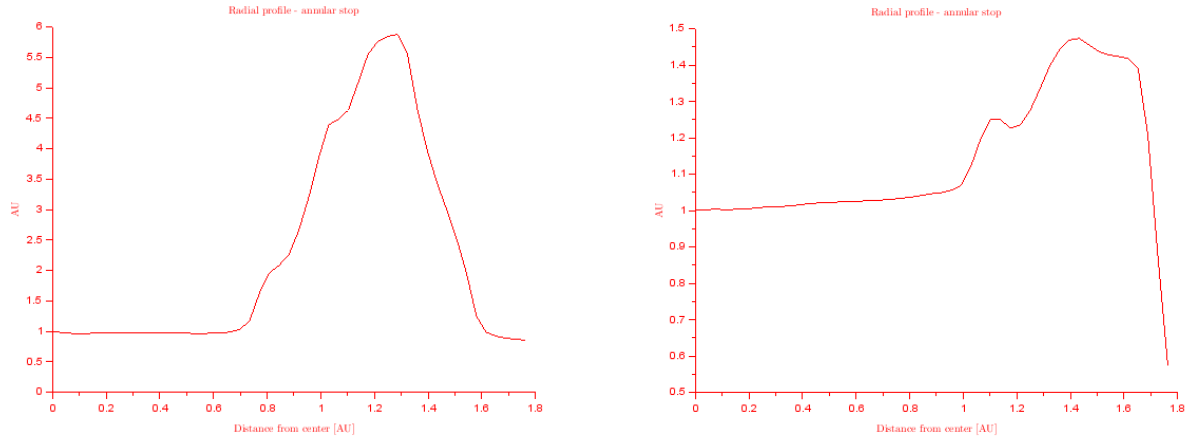

Figure 14 Average angular distribution without diffuser (left) and with diffuser (right).

Radiance uniformity

The radiance uniformity over the annular stop (spatial distribution) is lower than 10%. The angular uniformity is shown in the following picture with the case of no diffuser mounted on the system. Each picture corresponds to a position along the annular stop. The angular distribution is calculated as the radial average of the light distribution. The center of the distribution is calculated as the center of the outer circle of the distribution. This method gives nearly the same radial distribution, regardless the point considered over the annular stop.

The angular distribution can be improved as shown in the following picture by using a diffuser. In this case the ratio of the center to peak value is about 1.5, but the radiance is reduced by a factor of two.

The measurement on the IC configuration for the spatial uniformity over the aperture of the 1.0 AU case show a radiance uniformity equal to about 4%.

The measurement has been repeated for the larger aperture (0.5 AU) using a sampling of 0.1 mm along one direction and 2 mm along the vertical direction.

The resulting distribution is shown in Figure 15; each acquisition point has been obtained by averaging five acquisitions of 1 ms. The rms error has been calculated for each point leading to a relative error of few percent over the whole acquisition range.

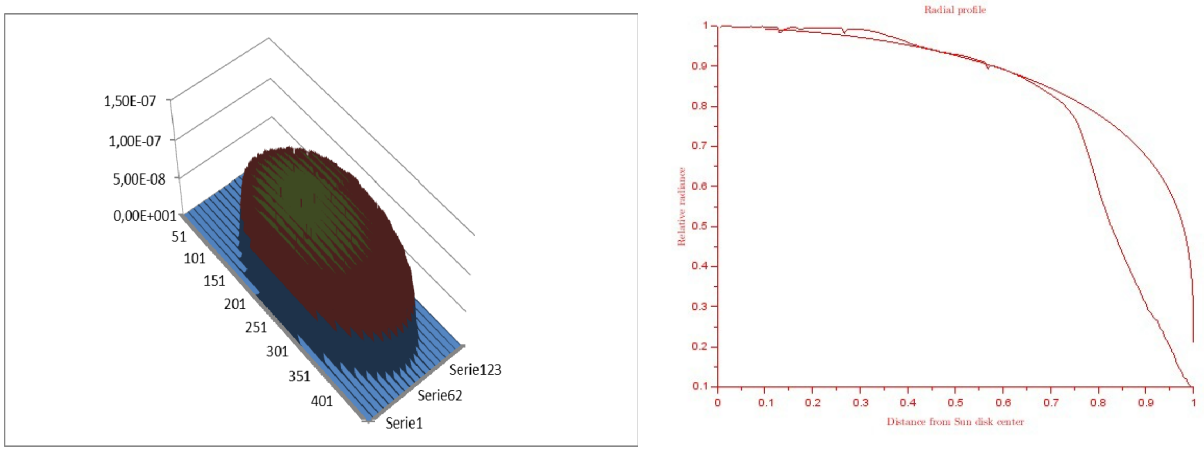

Figure 15 Radiance distribution, raw data (left) and resulting radial profile (right).

The data have been re-sampled to obtain the same spatial sampling over the two axis. The resulting interpolated distribution has been used to calculate the radial profile of the radiance in angle space, which is related to the spatial distribution by the focal length of the off-axis parabola. The resulting distribution is shown in Figure 15.

5. CONCLUSIONS

An illumination system for the stray-light measurement of the METIS coronagraph has been designed, assembled and tested. The system is able to provide in every operating condition a radiance level high enough to allow the stray-light measurement down to the tight rejection factor required by METIS and within few seconds of exposure time in ambient condition (no detector cooling required).

The angular and spatial calibration of the radiance gives the information needed to allow the comparison the measurements performed with ISVL with the expected results obtained through simulations.

REFERENCES

[1] Fineschi, S., "*Novel Optical Designs for Space Coronagraphs: inverted occulters and Lyot-stops"*, ICSO Proc. – International Conference on Space Optics, Rhodes, Greece (Oct. 4th – 8th, 2010).

[2] Naletto, G., Antonucci, E., Andretta, V., Battistelli, E., Cesare, S., Da Deppo, V., d'Angelo, F., Fineschi, S., Focardi, M., Lamy, P., Landini, F., Moses, D., Nicolini, G., Nicolosi, P., Pancrazzi, M., Pelizzo, M.G., Poletto, L., Romoli, M., Solanki, S., Spadaro, D., Teriaca, L., Uslenghi, M., Zangrilli, L., *"METIS, the Multi Element Telescope for Imaging and Spectroscopy for the Solar Orbiter Mission"*, ICSO Proc. – International Conference on Space Optics, Rhodes, Greece (Oct. 4th – 8th, 2010)

[3] Fineschi, S., Antonucci, E., Naletto, G., Romoli, M., Spadaro, D., Nicolini, G., Abbo, L., Andretta, V., Bemporad, A., Berlicki, A., Capobianco, G., Crescenzio, G., Da Deppo, V., Focardi, M., Landini, F., Massone, G., Malvezzi, M., Moses, J.D., Nicolosi, P., Pancrazzi, M., Pelizzo, M-G., Poletto, L., Schühle, U., Solanki, S.K., Telloni, D., Teriaca, L,, Uslenghi, M., "*METIS: a novel coronagraph design for the Solar Orbiter mission",* Proc. SPIE Vol. 8443, 84433H ·(2011)

[4] Verroi, E., Da Deppo, V., Naletto, G., Fineschi, S., Antonucci, E., *"Preliminary internal straylight analysis of the METIS instrument for the Solar Orbiter ESA mission"*, Proc. SPIE Vol. 8442, (2012)

[5] S. Fineschi, G. Crescenzio, G. Massone, G. Capobianco, L. Zangrilli, E. Antonucci, F. Anselmi, *"OPSys: Optical Payload Systems Facility for testing space coronagraphs"*, Proc. SPIE Vol. 8148, 31-41 (2011).

[6] Crescenzio, G., Fineschi, S., *"Stray light suppression analysis of the Space Optics Calibration Chamber (SPOCC)"*; INAF-Osservatorio Astronomico di Torino Technical Report n. 139 (2010). Website: www.oato.inaf.it/biblioteca/pdf/TechRep147_Crescenzio.pdf

[7] Fineschi, S., Antonucci, E., Romoli, M., Gardiol, D., Naletto, G., Giordano, S., Malvezzi, M., Da Deppo, V., Zangrilli, L., Noci, G., "*Ultraviolet and Visible-light Coronagraphic Imager (UVCI)for HERSCHEL (Helium Resonance Scattering in Corona & HELiosphere)",* Proc. SPIE Vol. 4853 pp. 162-171 (2003).

[8] Chuh, T.Y., *"Recent developments in infrared and visible imaging for astronomy, defense, and homeland security"*, Proc.SPIE Vol. 5563, pp. 19-34 (2004).

[9] M. Tordi, S. Fineschi, G. Crescenzio, *"The visible light source for METIS stray-light tests: preliminary design"*, Proc. SPIE Vol. 8862, pp. 15 (2013)